

## Verification of the 2D/1D Coupling 3D Transport Code TIGER with C5G7 Benchmarks

Wenbin Wu<sup>1</sup>, Qing Li<sup>1</sup>, Kan Wang<sup>2</sup>

1. Science and Technology on Reactor System Design Technology Laboratory, Nuclear Power Institute of China, Chengdu, 610213, China. wenbinwu@126.com
2. Department of Engineering Physics, Tsinghua University, Beijing, 100084, China

**Abstract** – TIGER is a 2D/1D coupling 3D transport code developed by Nuclear Power Institute of China based on large-scale parallel computation. It employs 2D domain-decomposed parallel Matrix MOC in the radial direction and 1D finite difference diffusion in the axial direction. 2D domain-decomposed parallel Matrix MOC is accelerated with multi-group and multi-domain coupled PGMRES algorithm. Generally, 2D planar problem are solved independently and parallel degree is natural in the axial direction. Combination of the parallel degrees of both radial and axial directions is used in TIGER to achieve the large-scale parallel computation. In this paper, a few variations of C5G7 benchmarks were created in the base of the published benchmarks. Reference results of these variations were provided by the Monte Carlo code RMC. To demonstrate the accuracy and efficiency of TIGER, C5G7 benchmarks and these relevant variations were calculated by TIGER, and the comparisons were made with the published results and Monte Carlo results.

### I. INTRODUCTION

For typical nuclear reactors, geometry is much heterogeneous in the radial direction while relatively homogenous in the axial direction. Due to this geometrical advantage, a number of 2D/1D coupling 3D neutron transport codes have been developed in recent years, such as CRX<sup>[1]</sup>, nTRACER<sup>[2]</sup>, and MPACT<sup>[3]</sup>. In 2D/1D methods, a 3D problem is transformed into a combination of 2D planar problems and 1D axial problems, which have a smaller computational burden than the original problem. 2D planar problems and 1D axial problems are coupled with axial and transverse leakage sources. Generally, these methods employ 2D MOC in the radial direction and 1D diffusion or 1D transport in the axial direction.

TIGER<sup>[4]</sup> is a 2D/1D coupling 3D transport code developed by Nuclear Power Institute of China based on large-scale parallel computation. TIGER employs 2D Matrix MOC in the radial direction and 1D finite difference diffusion method in the axial direction. Parallel degrees in both directions are combined via domain decomposition.

In this paper, a few variations of C5G7 benchmarks were created in the base of the published benchmarks. TIGER was verified by the C5G7 benchmarks and these relevant variations. The  $k_{eff}$  results of all cases were calculated by TIGER, and the comparisons were made with the benchmark results or Monte Carlo results. Additionally, comparisons of pin by pin powers were made for some cases.

The present paper is organized as follows. Section II describes in detail the methodologies of TIGER. Section III presents the description of C5G7 variations and the

numerical results. Section IV provides the summary and conclusions.

### II. THEORY

#### 1. 2D/1D Coupling Scheme

Starting from the 3D Boltzmann transport equation for a particular angle  $m$  and energy group  $g$ :

$$\xi_m \frac{\partial \psi_g(\mathbf{r}, \Omega_m)}{\partial x} + \eta_m \frac{\partial \psi_g(\mathbf{r}, \Omega_m)}{\partial y} + \mu_m \frac{\partial \psi_g(\mathbf{r}, \Omega_m)}{\partial z} + \Sigma_{t,g}(\mathbf{r}) \psi_g(\mathbf{r}, \Omega_m) = Q_g(\mathbf{r}, \Omega_m) \quad (1)$$

$$Q_g(\mathbf{r}, \Omega_m) = \frac{1}{4\pi} \sum_{g'=1}^G \Sigma_{s,g' \rightarrow g}(\mathbf{r}) \phi_{g'}(\mathbf{r}) + \frac{\chi_g}{4\pi k_{eff}} \sum_{g'=1}^G \nu \Sigma_{f,g' \rightarrow g}(\mathbf{r}) \phi_{g'}(\mathbf{r}) \quad (2)$$

where

$\psi_g(\mathbf{r}, \Omega_m)$  = angular flux of angle  $m$  and energy group  $g$

$\Sigma_{t,g}(\mathbf{r})$  = total cross section of energy group  $g$

$\Omega_m = (\xi_m, \eta_m, \mu_m)$  is the angle of angular flux

$\mathbf{r} = (x, y, z)$  is the position

$Q_g(\mathbf{r}, \Omega_m)$  = the sum of the fission and scattering sources.

Integrating Eq. (1) over a 2D plane axially and moving the axial streaming to the right hand side, the 2D transport equation for plane  $k$  is yielded as Eq. (3).

$$\xi_m \frac{\partial \Psi_{g,m,k}(x, y)}{\partial x} + \eta_m \frac{\partial \Psi_{g,m,k}(x, y)}{\partial y} + \Sigma_{t,g,k}(x, y) \Psi_{g,m,k}(x, y) = Q_{g,k}(x, y) - TL_{g,m,k}^{Axial}(x, y) \quad (3)$$

In Eq. (3), the axial leakage source is denoted by neutron currents at the top (T) and bottom (B) of each

plane as in Eq. (4). The axial leakage source is assumed to be isotropic.

$$TL_{g,m,k}^{Axial}(x,y) = \frac{1}{4\pi\Delta z_k} [J_{g,k}(z^T) - J_{g,k}(z^B)] \quad (4)$$

$TL_{g,m,k}^{Axial}(x,y)$  = the axial leakage source of plane  $k$

$\Delta z_k$  = the thickness of the plane  $k$

$J_{g,k}(z^T)$  = net current of the top surface of the plane  $k$

$J_{g,k}(z^B)$  = net current of the bottom surface of the plane  $k$

Eq. (3) is a transport equation of 2D heterogeneous planes, which are solved by 2D Matrix MOC. Then, cells are homogenized by the 2D solutions of the planar problems.

Similarly, integrating radially over homogenized cell  $p$ , we obtain 1D transport equation

$$\mu_m \frac{d\psi_{g,m}^p(z, \mu_m, \varphi_m)}{dz} + \Sigma_{t,g,p}(z) \psi_{g,m}^p(z, \mu_m, \varphi_m) = Q_g^p(z) - TL_{g,m,p}^{Radial}(z, \mu_m, \varphi_m) \quad (5)$$

where

$\Sigma_{t,g,p}(z)$  = the homogenized cross section of cell  $p$

$TL_{g,m,p}^{Radial}(z, \mu_m, \varphi_m)$  = the transverse leakage source of cell  $p$ .

For the transverse leakage source, isotropic assumption is also used, and it is expressed by net current as follows.

$$TL_{g,m,p}^{Radial}(z) = \frac{1}{2} \left( \frac{1}{\Delta x} (J_{g,x+}^p - J_{g,x-}^p) + \frac{1}{\Delta y} (J_{g,y+}^p - J_{g,y-}^p) \right) \quad (6)$$

where

$\Delta x \Delta y$  = side length of cell  $p$

$J_{g,i}^p$  = net current of  $i$  surface of cell  $p$ .

Adopting diffusion approximation and solving Eq. (5) by finite difference method, we yield Eq. (7).

$$\frac{1}{\Delta z} (J_{g,z+}^p - J_{g,z-}^p) + \Sigma_{t,g,p} \phi_{g,p} = \frac{\chi_g}{k_{eff}} \sum_{g'=1}^G (v \Sigma_f)_{g',p} \phi_{g'}^p + \sum_{g'=1}^G \Sigma_{s,g'-g,p} \phi_{g'}^p - \left( \frac{1}{\Delta x} (J_{g,x+}^p - J_{g,x-}^p) + \frac{1}{\Delta y} (J_{g,y+}^p - J_{g,y-}^p) \right) \quad (7)$$

Solving Eq. (3) and Eq. (7) alternately, and transferring transverse and axial leakage terms between them in the framework of 3D CMFD formulation, results of Eq. (1) can be obtained.

## 2. The Matrix Method of Characteristic and Spatial Domain Decomposition

In the 2D/1D coupling scheme, the principal computational burden mostly lies in the solution of 2D planar problems. The reason is that typical reactors are very heterogeneous in the radial direction, and neutron transport equations are essential. Therefore, the 2D transport solver is important for the accuracy and efficiency of the 2D/1D coupling methods. In this work, 2D planar problem Eq. (3) is solved by 2D Matrix MOC based on spatial domain decomposition.

Matrix MOC (MMOC)<sup>[5]</sup> was proposed by Dr. Zhang. In Matrix MOC, a linear algebraic equation system (Eq.(8)) represented by coefficient-matrix is formed by sweeping only once, and then solving the linear system takes the place of repeatedly characteristics sweeping.

$$\mathbf{A}x = \mathbf{B}q_f \quad (8)$$

In Eq. (8),  $\mathbf{A}$  and  $\mathbf{B}$  are coefficient-matrices with good numerical features, such as sparsity and symmetry.  $x$  is the vector containing scalar fluxes and angular fluxes at outer boundary in all energy groups.  $q_f$  is only the fission source, while the scattering source is embedded in matrix  $\mathbf{A}$ . Benefiting from the numerical features, the construction computation and memory demand of the coefficient-matrices can be reduced significantly.

Once the spatial domain is decomposed as in Fig. 1, Eq. (8) for the whole problem domain is changed into Eq. (9) and Eq. (10) for each subdomain, where  $\psi_{in}$  and  $\psi_{out}$  are incoming and outgoing angular fluxes at inner boundary,  $q_s$  is the scattering source and  $\mathbf{C} \mathbf{D} \mathbf{E} \mathbf{F}$  are corresponding matrices. Eq. (11) is the continuous boundary condition at inner boundary. Matrices  $\mathbf{C} \mathbf{D} \mathbf{E} \mathbf{F}$  have good numerical features, too.

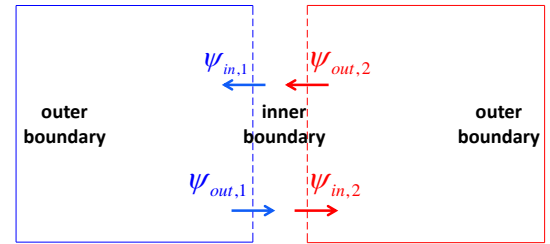


Fig. 1. Illustration of spatial domain decomposition

$$\mathbf{A}x = \mathbf{B}q_f + \mathbf{C}\psi_{in} \quad (9)$$

$$\psi_{out} = \mathbf{D}(q_s + q_f) + \mathbf{E}x + \mathbf{F}\psi_{in} \quad (10)$$

$$\psi_{in} = \psi_{out} \quad (11)$$

Eq. (9), Eq. (10), and Eq. (11) are fundamental equations of MMOC based on domain decomposition. As we can see, incoming angular fluxes at inner boundary  $\psi_{in}$  are unknown when each subdomain is solved independently and in parallel. Initial guesses of  $\psi_{in}$  and corresponding iterations are needed. In the ordinary way,  $\psi_{in}$  iteration is fundamentally the slow Jacobi iteration. When the whole problem is divided into finer subdomains, the iteration cost of  $\psi_{in}$  is significant. For this reason, we propose the multi-group and multi-domain coupled Parallel GMRES (MGMD PGMRES) algorithm to solve 2D planar problems with energy upscattering and domain decomposition.

### 3. The Multi-Group and Multi-Domain Coupled PGMRES Algorithm

Setting  $[x, \psi_{out}]^T$  in each subdomain as unknowns, Eq. (9) and Eq. (10) are transformed into Eq. (12). In Eq. (12), the scattering sources are all moved to the left hand side.

$$\begin{bmatrix} \mathbf{A} & \mathbf{0} \\ -\mathbf{E} & \mathbf{I} \end{bmatrix} \begin{bmatrix} x \\ \psi_{out} \end{bmatrix} - \begin{bmatrix} \mathbf{C}\psi_{in} \\ \mathbf{F}\psi_{in} \end{bmatrix} - \begin{bmatrix} \mathbf{0} \\ \mathbf{D}q_s \end{bmatrix} = \begin{bmatrix} \mathbf{B}q_f \\ \mathbf{D}q_f \end{bmatrix} \quad (12)$$

PGMRES is the parallel version of GMRES algorithm, one of the Krylov subspace iterative methods for linear systems. Like most Krylov methods, only multiplication operator of a matrix on a vector should be provided to the PGMRES interface. Specific to Eq. (12),  $[x, \psi_{out}]^T$  of each subdomain is input vector, and the left hand side represents the result of the multiplication operator, where  $\psi_{in}$  is got from the neighboring subdomain by communication according to the continuous boundary condition at inner boundary, i.e. Eq. (11).

In the MGMD PGMRES algorithm, convergence of iterations of  $\psi_{in}$  at inner boundaries is improved compared with the ordinary Jacobi iteration. In this work, the PGMRES implementation is from PETSc<sup>[6]</sup> library, which is flexible and friendly to the users with reverse communication interfaces and matrix-free data structure.

### 4. 1D Solver Embedded Into 3D CMFD

Moving the radial leakage term to the left hand side of Eq. (7), we get Eq. (13).

$$\begin{aligned} & \frac{1}{\Delta x} (J_{g,x+}^p - J_{g,x-}^p) + \frac{1}{\Delta y} (J_{g,y+}^p - J_{g,y-}^p) + \frac{1}{\Delta z} (J_{g,z+}^p - J_{g,z-}^p) \\ & + \sum_{i,g,p} \phi_{g,p}^p - \sum_{g=1}^G \sum_{s,g'-g,p} \phi_{g'}^p = \frac{\chi_g}{k_{eff}} \sum_{g'=1}^G (\nu \Sigma_f)_{g',p} \phi_{g'}^p \end{aligned} \quad (13)$$

Eq. (13) turns out to be the 3D CMFD equation. Thus, the 1D axial diffusion solver is embedded or hidden into the 3D CMFD formulation.

It should be noted that the 3D CMFD equation is decomposed completely both in radial and axial directions, making it rough to handle. Similarly as the domain-decomposed MMOC, MGMD PGMRES algorithm in matrix free mode is also used. The input vectors are the scalar fluxes of homogenized cells of each sub-domain. The left hand side of Eq. (13) represents the result of the matrix-vector multiplication operator. The matrix-vector multiplication operator is denoted by direct finite difference instead of explicit matrix. In other words, for the surface  $c + \frac{1}{2}$  in Fig. 2, the net current in Eq. (13) is expressed as Eq. (14).

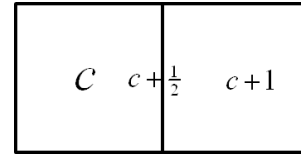


Fig. 2. Illustration of net current by direct finite difference

$$J_{c+\frac{1}{2},g,CMFD} = -\tilde{D}_{c+\frac{1}{2},g} (\phi_{c+1,g,CMFD} - \phi_{c,g,CMFD}) + \hat{D}_{c+\frac{1}{2},g} (\phi_{c+1,g,CMFD} + \phi_{c,g,CMFD}) \quad (14)$$

$$\tilde{D}_{c+\frac{1}{2},g} = \frac{2D_c D_{c+1}}{D_c \Delta x_{c+1} + D_{c+1} \Delta x_c} \quad (15)$$

$J_{c+\frac{1}{2},g,CMFD}$  = net current at surface  $c + \frac{1}{2}$

$\phi_{c,g,CMFD}$  = the CMFD scalar flux of cell  $c$

$\tilde{D}_{c+\frac{1}{2},g}$  = effective diffusion coefficient based on diffusion theory

$\hat{D}_{c+\frac{1}{2},g}$  = the current correction factor

$D_c$  = the diffusion coefficient of cell  $c$

$\Delta x_c$  = the length of cell  $c$ .

For surface  $c + \frac{1}{2}$  at the inner boundary resulting from the domain decomposition, cell  $c+1$  belongs to the neighboring sub-domain. Therefore, scalar flux  $\phi_{c+1,g,CMFD}$  is obtained by communication from neighboring process.

### 5. Large-scale Parallel Computation Model

In this 2D/1D coupling scheme, 2D planar problems are solved independently, and the axial parallel degree is natural. For the 2D planar problems, domain-decomposed MMOC is used, so the radial parallel degree exists.

Straightforwardly, large-scale parallel computation can be realized by combination of the parallel degrees of both radial and axial directions. According to the theory, TIGER code is developed.

In TIGER, each MPI process deals with a sub-domain of a 2D planar problem. All the processes are mapped into 3D structure based on the domain decomposition. Radial and axial MPI communicators are defined to manage the message passing. For typical PWR reactors, the height is about 3.5m, and there are about 157 assemblies. Dividing the 3D reactor into 30 planes in the axial direction, and each process dealing with 1/4 assembly, totally 18840 computing cores can be utilized.

The calculation flowchart of TIGER code is shown in Fig. 3.

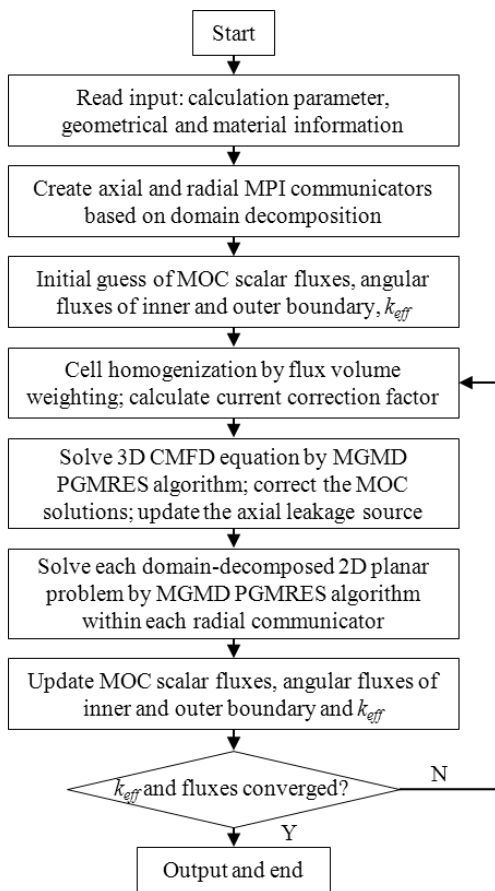


Fig. 3. Flowchart of 2D/1D coupling code TIGER

### III. NUMERICAL RESULTS

#### 1. Benchmark Description and Computational Condition

The C5G7 benchmarks [7,8] were published by the Organization for Economic Cooperation and Development Nuclear Energy Agency (OECD/NEA) to

test the ability of modern deterministic transport methods and codes to treat such reactor core problems without spatial homogenization. A seven group set of cross sections were collapsed from WIMS-AECL 69 group library by DRAGON. The seven group cross sections are transport corrected and isotropic scattering.

In 2003, the original benchmark specified a 2D and 3D problem. In 2005, a second benchmark was created as an extension of the first which included multiple control rod configurations and were more challenging. In these two benchmarks, fuel, gap, and cladding materials were homogenized into “Fuel-Clad Mix”. In 2015, a more heterogeneous modification [1] of C5G7 benchmark was proposed, in which claddings were attached. Furthermore, the realistic C5G7 benchmark was mirrored by the reflective bottom to be more practical.

The C5G7 benchmarks and relevant variations are analyzed using the TIGER code. The computational condition is: 6 polar angles in  $(0, \pi)$ , 32 azimuths in  $(0, 2\pi)$ , ray spacing  $\sim 0.01$  cm,  $\sim 30$  meshes in each fuel cell. The calculation platform is a cluster with Intel SandBridge E5-2670 CPU linked by Infinite band network.

#### 2. 2D C5G7 Problem

The benchmark model [7] consists of four  $17 \times 17$  PWR  $UO_2$ /MOX assemblies distributed in a checkerboard pattern, as shown in Fig. 4. The overall dimensions of the 2D configuration are  $64.26$  cm  $\times$   $64.26$  cm, while each assembly is  $21.42$  cm  $\times$   $21.42$  cm.

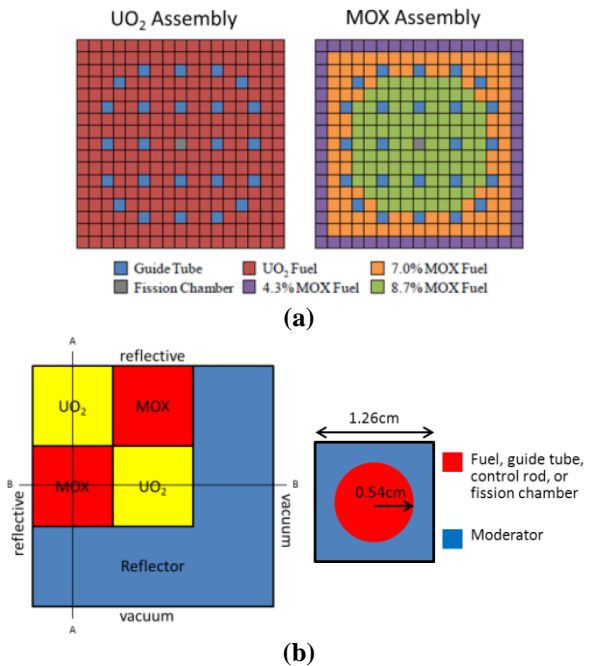


Fig. 4. Geometries of 2D C5G7 problem. (a) Assembly configuration, (b) Core and pin-cell configuration

The 2D benchmark model was established in a thickness of 1 cm slice with a reflective boundary on its top and bottom to form a 3D problem to be calculated by TIGER.

The mesh divisions of fuel cells and reflector cells are demonstrated in Fig. 5. As the interference effect between fuel and reflector are strong, finer mesh division is essential as in (b) of Fig. 5. If there is no special note, mesh divisions of following benchmarks are the same as Fig. 5.

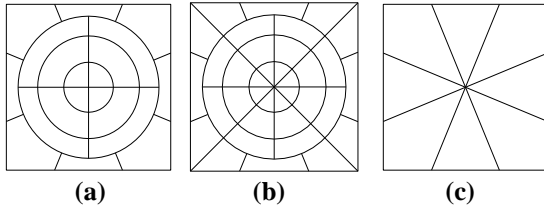


Fig. 5. Mesh division of C5G7 benchmarks with fuel-clad mix. (a) Fuel cells, (b) Fuel cells near reflector, (c) Reflector cells

The eighth symmetric reactor was calculated with 55 computer cores. The numerical results for 2D C5G7 benchmark are demonstrated in Table I. The  $k_{eff}$  and pin power distribution agree well with the benchmark results.

Table I. Numerical results of 2D C5G7 problem

$k_{eff}$ Error (pcm)	37
Assembly Power Error (%)	
Inner UO <sub>2</sub>	-0.035
MOX	0.050
Outer UO <sub>2</sub>	-0.031
Pin Power Error (%)	
Max. Power Pin	-0.052
Min. Power Pin	0.585
Max. Pin Power Error	0.966
Pin Power Distribution Error (%)	
Mean	0.197
RMS	0.265
MRE	0.162
Computational Time ( s )	7.15

### 3. The Original 3D C5G7 Problem

For the 3D configuration [7], the fuel assemblies are 192.78 cm in the z direction (as shown in Fig. 6) and an additional 21.42 cm water reflector is added axially. The z boundary conditions are reflected below and vacuum above.

10 planes were divided axially, and 100 computer cores were used. The computational time is 163.9 s. The numerical results for the original 3D C5G7 problem are

demonstrated in Table II, in which the TIGER results agree well with the benchmark results.

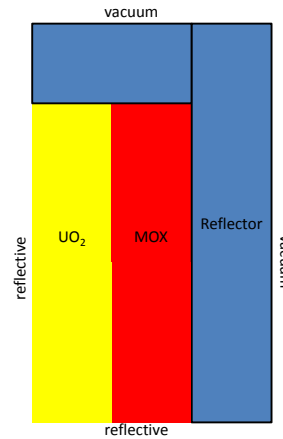


Fig. 6. Axial configuration of the original 3D C5G7 problem

Table II. Numerical results of the original 3D C5G7 problem

	Reference	TIGER	Error
$k_{eff}$	1.18381	1.18419	38 pcm
Inner UO <sub>2</sub>	492.9	492.6	-0.062%
MOX	211.8	211.8	0.018%
Outer UO <sub>2</sub>	139.6	139.7	0.094%
Max. Power Pin	2.5000	2.4962	-0.151%
Min. power pin	0.2300	0.2332	1.391%

### 4. The Extended 3D C5G7 Problem

For the extended benchmark [8], which includes control rods, the core geometry was reduced axially as shown in Fig. 7. Three cases named Unrodded, Rodded A, and Rodded B with different control rod positions were defined. 4 planes were divided axially, and 220 computer cores were used. The computational time is about 10.5 s.

Table III. Numerical results of the extended 3D C5G7 problem

Benchmark Case	Unrodded Case	Rodded A Case	Rodded B Case	
Eigenvalue Error (pcm)	-97	-62	-110	
Pin Power Error (%)	Max.	1.50	1.13	1.37
	Mean	0.26	0.22	0.28
	RMS	0.37	0.30	0.39
	MRE	0.18	0.18	0.24
Assembly Error (%)	Inner	-0.08	0.01	-0.23
	MOX	0.01	-0.03	0.11
	Outer	0.24	0.05	0.20
Computational Time (s)	10.2	10.4	10.7	

The numerical results for the extended 3D C5G7 problem are demonstrated in Table III. The eigenvalue

errors are separately -97 pcm, -62 pcm, -110 pcm for unrodded, rodded A, rodded B cases. For all three cases, the maximum axially integrated pin power error is 1.50%,

and the maximum slice integrated pin power error is 4.0% located at slice #3. These results agree well with the benchmark reference.

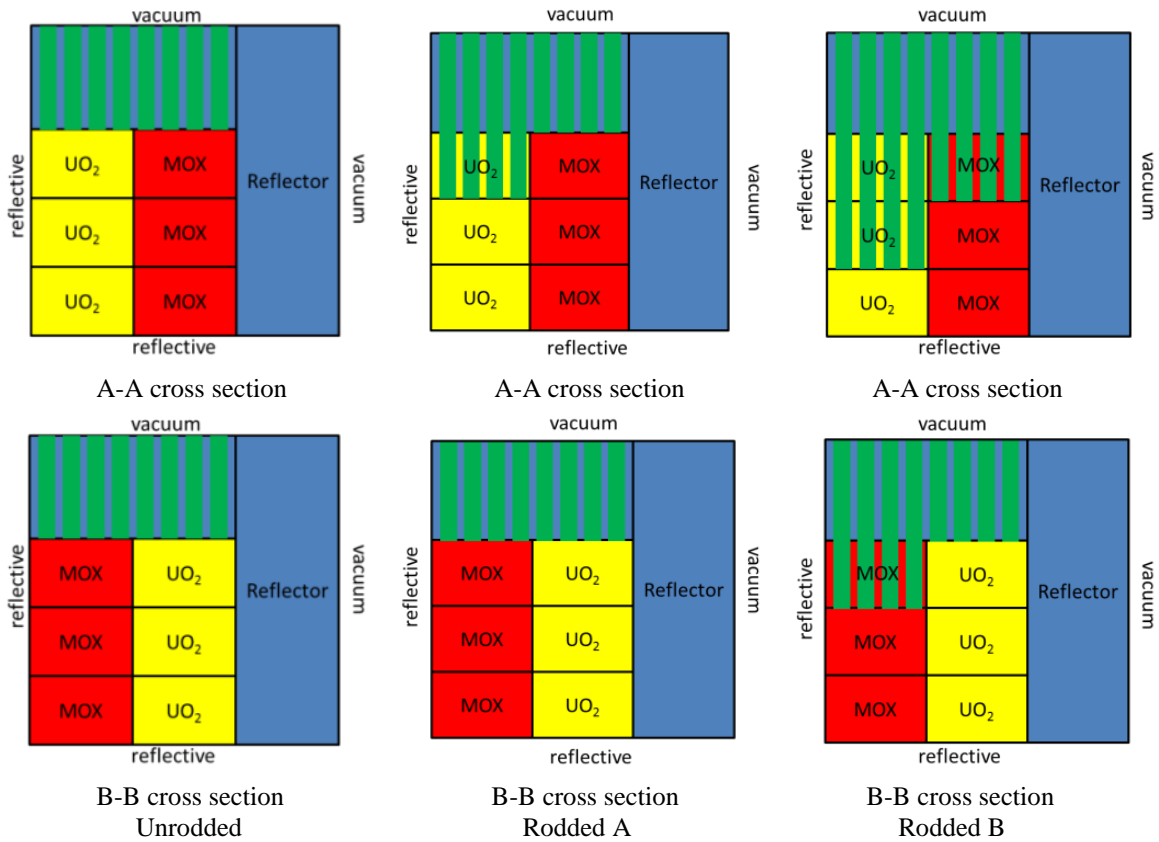


Fig. 7. Control rod configurations of the extended 3D C5G7 problem

### 5. The Modified 3D C5G7 Problem

For the modified 3D C5G7 problem<sup>[1]</sup>, claddings are attached explicitly to all fuel and guide tube pins as shown in Fig. 8, making it more heterogeneous. The computational conditions were the same as the extended one with the mesh division in Fig. 9. The computational time is about 14.5 s.



Fig. 8. Pin-cell of the modified 3D C5G7 problem

The  $k_{eff}$  results for the modified 3D C5G7 problem are demonstrated in Table IV, where the reference solutions were provided by Monte Carlo code RMC developed in

Tsinghua University. As this problem is more heterogeneous,  $k_{eff}$  errors of TIGER increase from ~100 pcm to ~150 pcm.

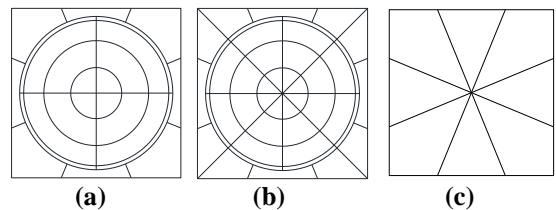


Fig. 9. Mesh division of C5G7 benchmarks with explicit clad. (a) Fuel cells, (b) Fuel cells near reflector, (c) Reflector cells

Table IV.  $k_{eff}$  results of the modified 3D C5G7 problem

	Reference	Error*, pcm	TIGER	Error, pcm
Unrodded	1.09928	$\pm 5$	1.09777	-151
Rodded A	1.08371	$\pm 5$	1.08250	-121
Rodded B	1.03234	$\pm 5$	1.03072	-162

\* RMC standard deviation

### 6. The Realistic 3D C5G7 Problem

The realistic 3D C5G7 problem was mirrored through the lower symmetry boundary of the extended and modified 3D C5G7 problems. To be realistic, no control rods were inserted from the bottom, as shown in Fig. 10 (taking Rodded B as an example).

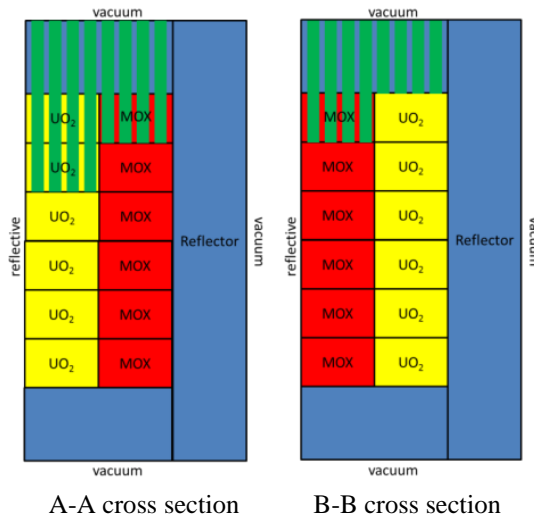


Fig. 10. Axial configuration of the realistic 3D C5G7 problem (Rodded B)

8 planes were divided axially, and 440 computer cores were used. The computational times are respectively ~11.0s and ~16.0s for the realistic extended and realistic modified problems. The  $k_{eff}$  results are demonstrated in Table V and Table VI. These results agree well with the reference results, with the maximum relative error 118 pcm and 173 pcm. As the realistic modified 3D C5G7 problems are more heterogonous, the  $k_{eff}$  errors are larger than those of the realistic extended 3D C5G7 problems.

Table V.  $k_{eff}$  results of the realistic extended 3D C5G7 problem with fuel-clad mix

	Reference	Error*, pcm	TIGER	Error, pcm
Unrodded	1.14387	$\pm 5$	1.14281	-106
Rodded A	1.13742	$\pm 5$	1.13636	-106
Rodded B	1.12166	$\pm 4$	1.12048	-118

Table VI.  $k_{eff}$  results of the realistic modified 3D C5G7 problem with explicit clad

	Reference	Error*, pcm	TIGER	Error, pcm
Unrodded	1.10033	$\pm 4$	1.09865	-168
Rodded A	1.09355	$\pm 5$	1.09194	-161
Rodded B	1.07739	$\pm 5$	1.07566	-173

\* RMC standard deviation

### IV. CONCLUSIONS

TIGER is a 2D/1D coupling whole-core transport code based on large-scale parallel computation, in which spatial domain decomposition was radially adopted and combined with the natural axial parallel degree. In this paper, TIGER code was verified with the C5G7 benchmarks and relevant variations. The overall accuracy of TIGER is encouraging, while the computation time is significantly reduced because of large-scale parallel computation. However, the errors increased for problems with much more heterogonous geometry. The reason might be the accuracy of 1D diffusion solvers in the axial direction.

Future work will include implementing 1D SN or 1D MOC solver in the axial direction to improve the accuracy and testing TIGER on larger clusters. For the relevant variations of C5G7 benchmarks, pin power distributions should be tallied by Monte Carlo code and comparison should be made to evaluate the accuracy of pin power distribution by TIGER.

### REFERENCES

1. S. YUK, "Whole-Core Transport Solutions with 2-D/1-D Fusion Kernel Via P-CMFD Acceleration and P-CMFD Embedding of Nonoverlapping Local/Global Iterations," *Nucl Sci Eng*, **181**,1, 1-16 (2015)
2. Y. S. JUNG, "Practical Numerical Reactor Employing Direct Whole Core Neutron Transport and Subchannel Thermal/Hydraulic Solvers," *Ann Nucl Energy*, **62**,357-374 (2013)
3. B. W. KELLEY, "2D/1D Approximations to the 3D NeutronTransportEquation.I: Theory,"*Proc. International Conference on Mathematics and Computational Methods Applied to Nuclear Science & Engineering(M&C 2013)*,Sun Valley, ID, United States, American Nuclear Society (2013) (CD-ROM).
4. W. WU. 2-D/1-D Method for Neutron Transport Based on Large-Scale Parallel Computation. *2014 ANS winter meeting*. CA, USA; 2014. (CD-ROM).
5. H. ZHANG, "Acceleration Technique Using Krylov Subspace Methods for 2D Arbitrary Geometry Characteristics Solver,"*Proc. PHYSOR 2010*, Pittsburgh, PA, United states,American Nuclear Society (2010) (CD-ROM).
6. S. BALAY, "PETSc Users Manual (Revision 3.4)," ANL-95/11, Argonne National Laboratory (2013)
7. E. E. LEWIS, "Benchmark On Deterministic Transport Calculations without Spatial Homogenisation," NEA/NSC/DOC(2003)16, OECD/NEA (2003)
8. E. E. LEWIS, "Benchmark On Deterministic Transport Calculations without Spatial Homogenisation-Mox Fuel Assembly 3-D Extension Case," NEA/NSC/DOC (2005)16, OECD/NEA (2005)